Research Article | Vol. 25, No. 22 | 30 Oct 2017 | OPTICS EXPRESS 27635
Optics EXPRESS

Photonic integrated circuit implementation of a sub-GHz-selectivity frequency comb filter for optical clock multiplication

ZIHAN GENG,[1,2] YIWEI XIE,[1] LEIMENG ZHUANG,[1,*] MAURIZIO BURLA,[3] MARCEL HOEKMAN,[4] CHRIS G. H. ROELOFFZEN,[4] AND ARTHUR J. LOWERY[1,2]

[1]*Electro-Photonics Laboratory, Electrical and Computer Systems Engineering, Monash University, Clayton, VIC3800, Australia*
[2]*Centre for Ultrahigh-bandwidth Devices for Optical Systems (CUDOS), Monash University, Clayton, VIC3800, Australia*
[3]*Institute of Electromagnetic Fields (IEF), ETH Zurich, 8092 Zurich, Switzerland*
[4]*LioniX International BV, PO Box 456, Enschede, 7500 AL, Netherlands*
**leimeng.zhuang@ieee.org*

Abstract: We report a photonic integrated circuit implementation of an optical clock multiplier, or equivalently an optical frequency comb filter. The circuit comprises a novel topology of a ring-resonator-assisted asymmetrical Mach-Zehnder interferometer in a Sagnac loop, providing a reconfigurable comb filter with sub-GHz selectivity and low complexity. A proof-of-concept device is fabricated in a high-index-contrast stoichiometric silicon nitride (Si_3N_4/SiO_2) waveguide, featuring low loss, small size, and large bandwidth. In the experiment, we show a very narrow passband for filters of this kind, i.e. a −3-dB bandwidth of 0.6 GHz and a −20-dB passband of 1.2 GHz at a frequency interval of 12.5 GHz. As an application example, this particular filter shape enables successful demonstrations of five-fold repetition rate multiplication of optical clock signals, i.e. from 2.5 Gpulses/s to 12.5 Gpulses/s and from 10 Gpulses/s to 50 Gpulses/s. This work addresses comb spectrum processing on an integrated platform, pointing towards a device-compact solution for optical clock multipliers (frequency comb filters) which have diverse applications ranging from photonic-based RF spectrum scanners and photonic radars to GHz-granularity WDM switches and LIDARs.

OCIS codes: (130.3120) Integrated optics devices; (230.5750) Resonators; (230.7390) Waveguides, planar; (060.0060) Fiber optics and optical communications; (060.5625) Radio frequency photonics.

References and links

1. M. A. Soto, M. Alem, M. Amin Shoaie, A. Vedadi, C.-S. Brès, L. Thévenaz, and T. Schneider, "Optical sinc-shaped Nyquist pulses of exceptional quality," Nat. Commun. **4**, 2898 (2013).
2. X. F. Yi, "Tb/s coherent optical OFDM systems enabled by optical frequency combs," J. Lightwave Technol. **28**, 2054–2061 (2010).
3. T. Bajraszewski, M. Wojtkowski, M. Szkulmowski, A. Szkulmowska, R. Huber, and A. Kowalczyk, "Improved spectral optical coherence tomography using optical frequency comb," Opt. Express **16**(6), 4163–4176 (2008).
4. Q. Wu and X. C. Zhang, "Free-space electro-optic sampling of terahertz beams," Appl. Phys. Lett. **67**, 3523–3525 (1995).
5. C. Y. She, J. R. Yu, H. Latifi, and R. E. Bills, "High-spectral-resolution fluorescence light detection and ranging for mesospheric sodium temperature measurements," Appl. Opt. **31**(12), 2095–2106 (1992).
6. A. G. Glenday, C. H. Li, N. Langellier, G. Chang, L. J. Chen, G. Furesz, A. A. Zibrov, F. Kärtner, D. F. Phillips, D. Sasselov, A. Szentgyorgyi, and R. L. Walsworth, "Operation of a broadband visible-wavelength astro-comb with a high-resolution astrophysical spectrograph," Optica **2**, 250–254 (2015).
7. D. F. Phillips, A. G. Glenday, C. H. Li, C. Cramer, G. Furesz, G. Chang, A. J. Benedick, L. J. Chen, F. X. Kärtner, S. Korzennik, D. Sasselov, A. Szentgyorgyi, and R. L. Walsworth, "Calibration of an astrophysical spectrograph below 1 m/s using a laser frequency comb," Opt. Express **20**(13), 13711–13726 (2012).
8. M. W. Graham, S. F. Shi, D. C. Ralph, J. Park, and P. L. McEuen, "Photocurrent measurements of supercollision cooling in graphene," Nat. Phys. **9**, 103–108 (2013).
9. N. Dudovich, D. Oron, and Y. Silberberg, "Single-pulse coherently controlled nonlinear Raman spectroscopy and microscopy," Nature **418**(6897), 512–514 (2002).

#303073 https://doi.org/10.1364/OE.25.027635
Journal © 2017 Received 9 Aug 2017; revised 13 Oct 2017; accepted 20 Oct 2017; published 25 Oct 2017

Optics EXPRESS

10. O. Gerstel, M. Jinno, A. Lord, and S. J. Ben Yoo, "Elastic optical networking: a new dawn for the optical layer," IEEE Commun. Mag. **50**, S12–S20 (2012).
11. T. A. Liu, N. R. Newbury, and I. Coddington, "Sub-micron absolute distance measurements in sub-millisecond times with dual free-running femtosecond Er fiber-lasers," Opt. Express **19**(19), 18501–18509 (2011).
12. B. R. Washburn, S. A. Diddams, N. R. Newbury, J. W. Nicholson, M. F. Yan, and C. G. Jørgensen, "Phase-locked, erbium-fiber-laser-based frequency comb in the near infrared," Opt. Lett. **29**(3), 250–252 (2004).
13. H. Murata, A. Morimoto, T. Kobayashi, and S. Yamamoto, "Optical pulse generation by electrooptic-modulation method and its application to integrated ultrashort pulse generators," IEEE J. Sel. Top. Quantum Electron. **6**, 1325–1331 (2000).
14. Y. Cheng, X. Luo, J. Song, T. Y. Liow, G. Q. Lo, Y. Cao, X. Hu, X. Li, P. H. Lim, and Q. J. Wang, "Passively mode-locked III-V/silicon laser with continuous-wave optical injection," Opt. Express **23**(5), 6392–6399 (2015).
15. S. Uvin, S. Keyvaninia, F. Lelarge, G. Duan, B. Kuyken, and G. Roelkens, "Narrow line width frequency comb source based on an injection-locked III–V-on-silicon mode-locked laser," Opt. Express **24**, 5277–5286 (2016).
16. V. Moskalenko, S. Latkowski, S. Tahvili, T. de Vries, M. Smit, and E. Bente, "Record bandwidth and sub-picosecond pulses from a monolithically integrated mode-locked quantum well ring laser," Opt. Express **22**(23), 28865–28874 (2014).
17. E. Bente, S. Latkowski, V. Moskalenko, M. Llorens-Revul, S. Tahvili, and K. Williams, "Mode-locked lasers in InP photonic integrated circuits," in *Optoelectronics, Photonic Materials and Devices Conference* (OPTO, 2017), pp. 101230F.
18. S. B. Papp, K. Beha, P. D. Haye, F. Quinlan, H. Lee, K. J. Vahala, and S. A. Diddams, "Microresonator frequency comb optical clock," Optica **1**, 10–14 (2014).
19. T. Herr, V. Brasch, J. D. Jost, C. Y. Wang, N. M. Kondratiev, M. L. Gorodetsky, and T. J. Kippenberg, "Temporal solitons in optical microresonators," Nat. Photonics **8**, 145–152 (2014).
20. X. L. Wang, J. Ding, W. J. Ni, C. S. Guo, and H. T. Wang, "Generation of arbitrary vector beams with a spatial light modulator and a common path interferometric arrangement," Opt. Lett. **32**(24), 3549–3551 (2007).
21. J. Schröder, M. A. F. Roelens, L. B. Du, A. J. Lowery, S. Frisken, and B. J. Eggleton, "An optical FPGA: reconfigurable simultaneous multi-output spectral pulse-shaping for linear optical processing," Opt. Express **21**(1), 690–697 (2013).
22. W. Bogaerts, D. Taillaert, B. Luyssaert, P. Dumon, J. Van Campenhout, P. Bienstman, D. Van Thourhout, R. Baets, V. Wiaux, and S. Beckx, "Basic structures for photonic integrated circuits in Silicon-on-insulator," Opt. Express **12**(8), 1583–1591 (2004).
23. C. R. Doerr, "Silicon photonic integration in telecommunications," Front. Phys. **3**, 37 (2015).
24. M. J. R. Heck, J. F. Bauters, M. L. Davenport, J. K. Doylend, S. Jain, G. Kurczveil, S. Srinivasan, Y. Tang, and J. E. Bowers, "Hybrid silicon photonic integrated circuit technology," IEEE J. Sel. Top. Quantum Electron. **19**, 6100117 (2013).
25. C. G. H. Roeloffzen, L. Zhuang, C. Taddei, A. Leinse, R. G. Heideman, P. W. L. van Dijk, R. M. Oldenbeuving, D. A. I. Marpaung, M. Burla, and K.-J. Boller, "Silicon Nitride microwave photonic circuits," Opt. Express **21**(19), 22937–22961 (2013).
26. K. Worhoff, R. G. Heideman, A. Leinse, and M. Hoekman, "TriPleX: a versatile dielectric photonic platform," Adv. Opt. Technol. **4**, 189–207 (2015).
27. M. Smit, J. van der Tol, and M. Hill, "Moore's law in photonics," Laser Photonics Rev. **6**, 1–13 (2012).
28. L. A. Coldren, S. W. Corzine, and M. L. Masanovic, *Diode Lasers and Photonic Integrated Circuits* (Wiley 2012).
29. L. Zhuang, C. G. H. Roeloffzen, M. Hoekman, K. J. Boller, and A. J. Lowery, "Programmable photonic signal processor chip for radiofrequency applications," Optica **2**, 854–859 (2015).
30. L. Zhuang, M. Hoekman, W. P. Beeker, A. Leinse, R. G. Heideman, P. W. L. van Dijk, and C. G. H. Roeloffzen, "Novel low-loss waveguide delay lines using Vernier ring resonators for on-chip multi-λ microwave photonic signal processors," Laser Photonics Rev. **7**, 994–1002 (2013).
31. C. K. Madsen and J. H. Zhao, Optical Filter Design and Analysis: A Signal Processing Approach (Wiley, 1999).
32. L. Chrostowski, X. Wang, J. Flueckiger, Y. Wu, Y. Wang, and S. T. Fard, "Impact of fabrication non-uniformity on chip-scale silicon photonic integrated circuit," in *Optical Fiber Communications Conference* (OFC, 2014), pp. Th1C.1.
33. O. Schwelb, "Transmission, group delay, and dispersion in single-ring optical resonators and add/drop filters-a tutorial overview," J. Lightwave Technol. **22**, 1380–1394 (2004).
34. F. Morichetti, C. Ferrari, A. Canciamilla, and A. Melloni, "The first decade of coupled resonator optical waveguides bringing slow light to applications," Laser Photonics Rev. **6**, 74–96 (2012).
35. M. S. Rasras, D. M. Gill, S. S. Patel, K. Y. Tu, Y. K. Chen, A. E. White, A. T. S. Pomerence, D. N. Carothers, M. J. Grove, D. K. Sparacin, J. Michel, M. A. Beals, and L. C. Kimerling, "Demonstration of a fourth-order pole-zero optical filter integrated using CMOS processes," J. Lightwave Technol. **25**, 87–92 (2007).
36. P. Orlandi, F. Morichetti, M. J. Strain, M. Sorel, P. Bassi, and A. Melloni, "Photonic integrated filter with widely tunable bandwidth," J. Lightwave Technol. **32**, 897–907 (2014).
37. R. Rudnick, A. Tolmachev, D. Sinefeld, O. Golani, S. Ben-Ezra, M. Nazarathy, and D. M. Marom, "Sub-banded/single-sub-carrier drop-demux and flexible spectral shaping with a fine resolution photonic processor," in *European Conference on Optical Communications* (ECOC, 2014), pp. PD.4.1.

Optics EXPRESS

38. T. Goh, M. Itoh, H. Yamazaki, T. Saida, and T. Hashimoto, "Optical Nyquist-filtering multi/demultiplexer with PLC for 1-Tb/s class super-channel transceiver," in *Optical Fiber Communications* (OFC, 2015), pp. Tu3A.5.
39. L. Zhuang, D. Marpaung, M. Burla, W. Beeker, A. Leinse, and C. Roeloffzen, "Low-loss, high-index-contrast Si_3N_4/SiO_2 optical waveguides for optical delay lines in microwave photonics signal processing," Opt. Express **19**(23), 23162–23170 (2011).
40. T. Zhu, Y. W. Hu, P. Gatkine, S. Veilleux, J. Bland-Hawthorn, and M. Dagenais, "Ultra-broadband high coupling efficiency fiber-to-waveguide coupler using Si_3N_4/SiO_2 waveguides on silicon," IEEE Photonics J. **8**, 1 (2016).
41. P. Dong, N. N. Feng, D. Feng, W. Qian, H. Liang, D. C. Lee, B. J. Luff, T. Banwell, A. Agarwal, P. Toliver, R. Menendez, T. K. Woodward, and M. Asghari, "GHz-bandwidth optical filters based on high-order silicon ring resonators," Opt. Express **18**(23), 23784–23789 (2010).
42. H. Yu, M. Chen, P. Li, S. Yang, H. Chen, and S. Xie, "Silicon-on-insulator narrow-passband filter based on cascaded MZIs incorporating enhanced FSR for downconverting analog photonic links," Opt. Express **21**(6), 6749–6755 (2013).
43. D. X. Xu, A. Delâge, R. McKinnon, M. Vachon, R. Ma, J. Lapointe, A. Densmore, P. Cheben, S. Janz, and J. H. Schmid, "Archimedean spiral cavity ring resonators in silicon as ultra-compact optical comb filters," Opt. Express **18**(3), 1937–1945 (2010).
44. S. Ibrahim, N. K. Fontaine, S. S. Djordjevic, B. Guan, T. Su, S. Cheung, R. P. Scott, A. T. Pomerene, L. L. Seaford, C. M. Hill, S. Danziger, Z. Ding, K. Okamoto, and S. J. Yoo, "Demonstration of a fast-reconfigurable silicon CMOS optical lattice filter," Opt. Express **19**(14), 13245–13256 (2011).
45. J. S. Fandiño, P. Muñoz, D. Doménech, and J. Capmany, "A monolithic integrated photonic microwave filter," Nat. Photonics **11**, 124–129 (2016).
46. R. S. Guzzon, E. J. Norberg, J. S. Parker, L. A. Johansson, and L. A. Coldren, "Integrated InP-InGaAsP tunable coupled ring optical bandpass filters with zero insertion loss," Opt. Express **19**(8), 7816–7826 (2011).
47. E. J. Norberg, R. S. Guzzon, J. S. Parker, L. A. Johansson, and L. A. Coldren, "Programmable photonic microwave filters monolithically integrated in InP–InGaAsP," J. Lightwave Technol. **29**, 1611–1619 (2011).
48. N. Hosseini, R. Dekker, M. Hoekman, M. Dekkers, J. Bos, A. Leinse, and R. Heideman, "Stress-optic modulator in TriPleX platform using a ezoelectric lead zirconate titanate (PZT) thin film," Opt. Express **23**(11), 14018–14026 (2015).

1. Introduction

To date, optical clock signals (periodically pulsed signals) with the spectrum of a frequency comb have enabled a number of industrial applications, such as data carrier for fiber-optic communications and networks [1,2], optical coherence tomography in medical diagnosis [3], free-space communications in defense [4], light detection and ranging (LIDAR) for topography and airborne observatory [5], astrocombs [6,7], photocurrent mapping [8] and Raman spectroscopy [9] in material science. In practice, introducing control of the repetition rate of the clock signal will greatly benefit these applications in terms of system flexibility and potential for wide-spread deployment. When applied for optical sampling in communication systems, for example, sampling rate adaptability is a useful technique associated with variable channel symbol rate in next generation elastic optical communication networks [10]. For LIDAR systems, the optical clock rate variability allows for optimum detection of objects at different distances or with different reflections [11].

Conventionally, an optical clock signal with a frequency comb spectrum can be generated using a fiber-based resonance cavity [12] or a serial cascade of multiple electro-optic modulators [13]. From a practical perspective, on-chip implementations of optical clock sources, e.g. integrated mode-locked lasers (MLLs) [14–17] and optically-pumped nonlinear micro-cavities [18,19], are highly desirable for many applications as an ultimately stable and compact solution for providing high quality pulses at low power consumption. They are excellent candidates for generating short optical pulses at high repetition rates, overcoming the limitation of fibers on cavity length. Also importantly, they can be constructed using the common semiconductor materials and processes for photonic integrated circuits (PICs), and are therefore expected to serve as key building blocks for creating complex optical functions on the chip scale. However, it is difficult to incorporate comb spacing variation, i.e. clock rate variation, in such sources due to the fixed device dimensions. An effective solution for this drawback is to use external optical comb filters. In principle, spatial light modulators are a straightforward approach to synthesize arbitrary filter shapes [20]. However, this approach

Optics EXPRESS

requires a combination of free-space optical devices which typically have a spectral resolution about 10 GHz [21] and needs critical control of stability.

As an alternative approach, interferometric filters implemented in PICs open a path for practical solutions. PIC-based filters not only enjoy the general advantages inherent to the PIC technologies [22–28] such as small size, low weight, and low power consumption (small SWaP), ultimate stability and control precision, and strong potential for low-cost volume fabrication, but also offer great design flexibility and the possibility to be incorporated in programmable signal processors [29,30]. However, such filters conventionally suffer from a tradeoff between the key performance metrics such as operation bandwidth, circuit complexity, insertion loss, and the chip size. In particular, the feature of sub-GHz frequency selectivity requires significant waveguide path lengths, e.g. in the order of a centimeter or longer [31]. In fact, this requirement severely affects PICs using high-index-contrast waveguides such as silicon materials [22–26] and III-V semiconductors [27,28], which are being widely investigated in both academia and industry because of their intrinsic superiority in device compactness and function diversity over their low-index-contrast counterparts. Typically, filters using such waveguides are more susceptible to fabrication imperfections that affect the waveguide geometry and uniformity [32], causing degradation in key performance metrics, i.e. higher waveguide loss and reduced operation bandwidth. In addition, waveguide materials with high nonlinearity and dispersion such as silicon on insulator [22] and indium phosphide [27] may give rise to significant phase errors between the waveguide paths, particularly with long waveguides, which limits the filter performance.

Here, we report a new PIC implementation of an optical clock multiplier. It comprises of a novel topology of a ring-resonator-assisted asymmetric Mach-Zehnder interferometer (A-MZI) incorporated in a Sagnac loop, providing a reconfigurable comb filter with sub-GHz frequency selectivity and low complexity. A proof-of-concept device is fabricated in a stoichiometric Si_3N_4/SiO_2 waveguide, featuring low loss, small size, and large bandwidth. As additional features, this circuit topology provides a promising solution for optical comb filters that have significantly lower requirement for control precision than conventional ring resonator-based filters [33–36] and have a 2-orders-of-magnitude advantage in size when compared with tapped-delay-line filters [37,38].

2. Design principle

Figure 1(a) shows the novel filter topology. The A-MZI has identical ring resonators attached to both of its arms, and has Port 3 and 4 interconnected forming a Sagnac loop. The coupling between the ring resonators and the A-MZI is implemented using 2-by-2 tunable couplers [29,30]. As an important part of the filter reconfigurability, each ring resonator can be completely decoupled from the A-MZI when its coupling coefficient is set to zero. In effect, this enables the synthesis of a variety of filter transfer functions, by simply choosing a different number of ring resonators. The Sagnac loop in the filter serves as a mirror which reflects an input lightwave (e.g. from Port 1) so that it passes the A-MZI twice in opposite directions. To derive the filter transfer function, an equivalent lattice-structured circuit topology can be used as shown in Fig. 1(b). In this topology, the filter reduces to a 1-dimensional network of two identical 2-by-2-port sections, i.e. two A-MZIs with one being a vertically inverted version of the other, which can be described using a transfer matrix [31]. The A-MZIs have an arm-length difference equal to half of the ring resonator's roundtrip length, the time delay and corresponding spectral period of which define the unit delay, $\Delta\tau$, (minimum delay difference between the optical paths) and the free spectral range (FSR) of the A-MZI, Δf_{FSR}, respectively.

Optics EXPRESS

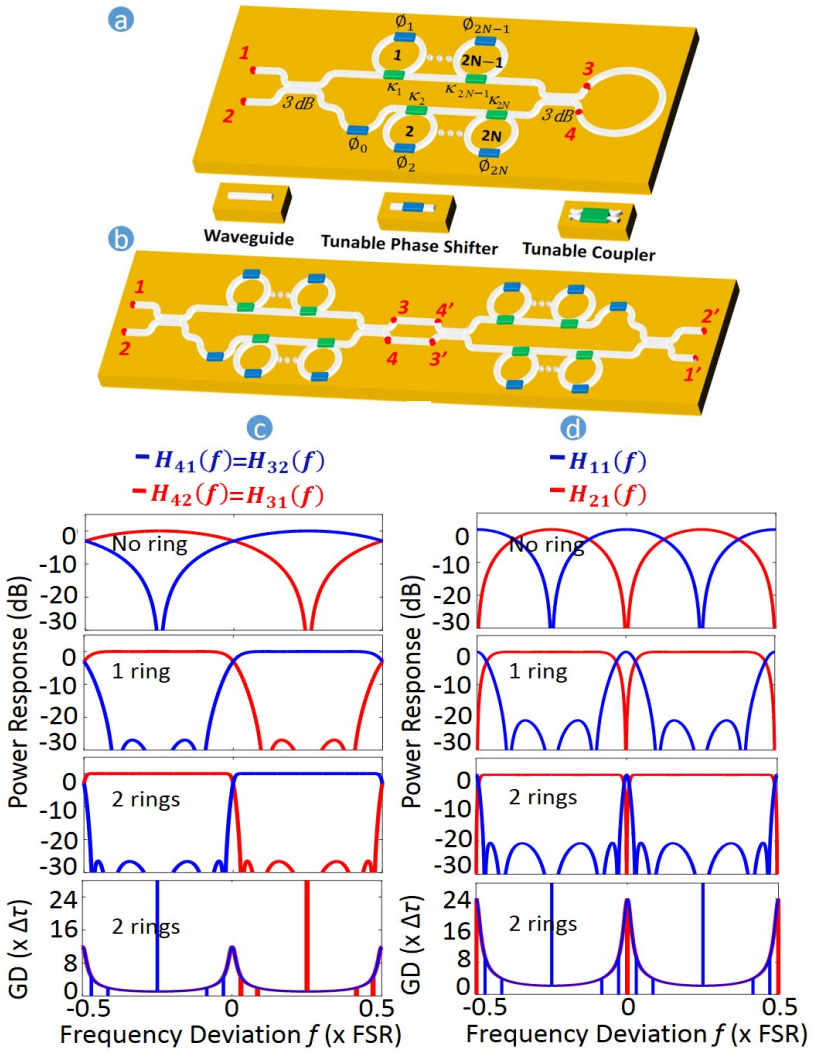

Fig. 1. (a) A schematic of the novel filter topology, (b) an equivalent lattice-structured circuit, (c) an illustration of the interleaving Chebyshev Type II filter shapes and group delays (GDs) of an A-MZI, (d) corresponding filter shapes and GDs at the outputs of the novel filter topology in (a).

The transfer matrix of an A-MZI, in the case that it stands alone, is given by

$$\begin{bmatrix} H_{31}(f) & H_{41}(f) \\ H_{32}(f) & H_{42}(f) \end{bmatrix} = \begin{bmatrix} H_{1'3'}(f) & H_{1'4'}(f) \\ H_{2'3'}(f) & H_{2'4'}(f) \end{bmatrix} = \eta \begin{bmatrix} \frac{\sqrt{2}}{2} & -\mathrm{j}\frac{\sqrt{2}}{2} \\ -\mathrm{j}\frac{\sqrt{2}}{2} & \frac{\sqrt{2}}{2} \end{bmatrix} \begin{bmatrix} \prod_{n=1,3,5\ldots}^{2N\pm1} R_n(f) & 0 \\ 0 & D(f)\prod_{n=2,4,6\ldots}^{2N} R_n(f) \end{bmatrix} \begin{bmatrix} \frac{\sqrt{2}}{2} & -\mathrm{j}\frac{\sqrt{2}}{2} \\ -\mathrm{j}\frac{\sqrt{2}}{2} & \frac{\sqrt{2}}{2} \end{bmatrix} \tag{1}$$

with

$$D(f) = te^{-\mathrm{j}2\pi f/\Delta f_{\mathrm{FSR}}} e^{-\mathrm{j}\phi_0} \tag{2}$$

Optics EXPRESS

and

$$R_n(f) = \frac{\sqrt{1-\kappa_n} - t^2 e^{-j4\pi f/\Delta f_{FSR}} e^{-j\phi_n}}{1-\sqrt{1-\kappa_n}\, t^2 e^{-j4\pi f/\Delta f_{FSR}} e^{-j\phi_n}}. \tag{3}$$

in which $D(f)$ and $R(f)$ describe the inter-arm delay line and ring resonator, respectively, with t the amplitude factor determined by the waveguide loss of a unit delay length, ϕ_n the tunable phase shift, κ_n the power coupling coefficient, and η a complex coefficient describing the overall insertion loss and phase shift of the A-MZI. Importantly, such an A-MZI is able to synthesize a spectral interleaving pair of Chebyshev Type II filters featuring equal-ripple stopbands [31] at the two complementary outputs. Figure 1(c) demonstrates such filter shapes for three cases where different numbers of ring resonators are coupled to the A-MZI. The corresponding filter coefficients are shown in Table 1. Based on this, the overall transfer matrix of the entire lattice-structured network is given by

$$\begin{aligned}\begin{bmatrix} H_{2'1}(f) & H_{2'2}(f) \\ H_{1'1}(f) & H_{1'2}(f) \end{bmatrix} &= \begin{bmatrix} H_{31}(f) & H_{32}(f) \\ H_{41}(f) & H_{42}(f) \end{bmatrix} \begin{bmatrix} H_{2'4'}(f) & H_{2'3'}(f) \\ H_{1'4'}(f) & H_{1'3'}(f) \end{bmatrix} \\ &= \begin{bmatrix} H_{31}(f)H_{2'4'}(f) + H_{32}(f)H_{1'4'}(f) & H_{31}(f)H_{2'3'}(f) + H_{32}(f)H_{1'3'}(f) \\ H_{41}(f)H_{2'4'}(f) + H_{42}(f)H_{1'4'}(f) & H_{41}(f)H_{2'3'}(f) + H_{42}(f)H_{1'3'}(f) \end{bmatrix}. \end{aligned} \tag{4}$$

Then, by combining Eqs. (1) and (4), the transfer matrix of the novel filter topology in Fig. 1(a) results to be

$$\begin{bmatrix} H_{11}(f) \\ H_{21}(f) \end{bmatrix} = \begin{bmatrix} H_{22}(f) \\ H_{12}(f) \end{bmatrix} = \begin{bmatrix} 2H_{31}(f)H_{41}(f) \\ H_{31}(f)H_{42}(f) + H_{41}(f)H_{32}(f) \end{bmatrix}. \tag{5}$$

Figure 1(d) demonstrates the filter shapes of $H_{11}(f)$ and $H_{21}(f)$, which are a complementary pair. In association with the spectral periodicity of the device, $H_{11}(f)$ provides a narrow-passband optical comb filter with reconfigurable bandwidth. The spectral passbands and similarly shaped group delays repeat themselves at a frequency interval (spectral period) equal to half of the A-MZI's FSR. This is because for $H_{11}(f)$ an input lightwave will sequentially pass two interleaving filter shapes of the A-MZI where the passband overlapping occurs at an interval of half FSR (Fig. 1(c)).

Table 1. Circuit parameters for the filter shapes in Fig. 1

	κ_1	κ_2	ϕ_0*	ϕn
No ring	0	0	$\epsilon [0, \pi]$	$\phi_0 + \pi$
1 ring	0.78	0	$\epsilon [0, \pi]$	$\phi_0 + \pi$
2 rings	0.89	0.35	$\epsilon [0, \pi]$	$\phi_0 + \pi$

* $\phi_0 \in [0, \pi]$ allows a tuning range of the filter-passband center frequency equal to the passband interval.

Regarding this filter property, Fig. 2(a) shows the filter passband bandwidths relative to the interval as a function of the number of ring resonators. From a practical viewpoint, using two ring resonators in our comb filter provides both excellent frequency selectivity and a low circuit complexity (a low number of building blocks such as delay lines, couplers, and tuning elements). Figure 2(b) shows the implementation advantages of our comb filter over several conventional filter topologies. In comparison, similar passband characteristics will require 81 taps for a tapped-delay-line filter. Such a large number of taps (delay lines) implies a requirement for a 2-orders-of-magnitude larger chip area and tens of times longer waveguides. As a result, the fabrication of such a filter will be more prone to severe issues of wafer uniformity and waveguide loss that lead to poor filter performance or total functional failure. Alternatively, conventional ring resonator-based topologies such as add-drop rings [33,34] and ring resonator-assisted Mach-Zehnder interferometers (RAMZIs) [35,36] feature similar circuit complexity. However, these will require the ring resonators to operate with

Optics EXPRESS

much higher quality factors (shown by much lower κ in Fig. 2(b)) to provide comparable filter passband characteristics. As a result, the filter performance and stability of the ring resonator is more sensitive to ambient disturbances and therefore will require more precise control during operation.

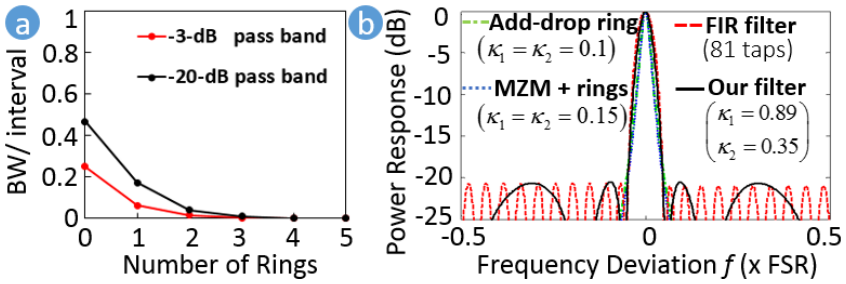

Fig. 2. (a) Calculations of filter passband bandwidth relative to interval as a function of the number of ring resonators. (b) Passband comparison between different filter designs, i.e. a tapped-delay-line (FIR) filter with 81 taps, a serial cascade of two add-drop ring resonators, and a serial cascade of two RAMZIs.

3. Device description

Recent advances in PIC technology has demonstrated a Si_3N_4/SiO_2 waveguide platform (TriPleX^{TM}, proprietary to Lionix B.V., The Netherlands) [26,39] that provides not only a low waveguide propagation loss of < 0.1 dB/cm at a bend radius of 70 μm or larger (smaller bend radii may also be used for particular applications, but raising a trade-off with noticeable effect of bend loss), but also a low wavelength dispersion at 1550 nm which is highly promising for fabricating C-band telecommunication devices. Using this waveguide, a proof-of-concept filter was fabricated for the experimental verification, a microphotograph of which is shown in Fig. 3(a).

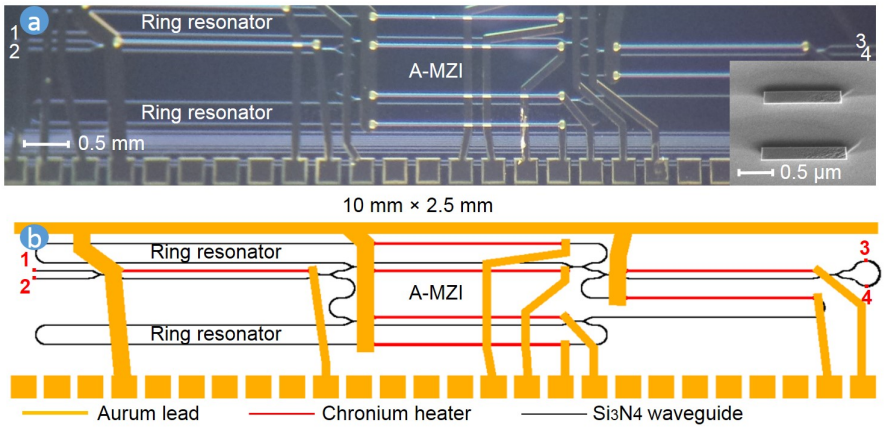

Fig. 3. (a) A photomicrograph of a fabricated chip. Inset: a scanning electron microscope (SEM) photograph of the waveguide cross-section. (b) The chip mask layout design.

As shown in the inset of Fig. 3(a), the waveguide consists of two strips of Si_3N_4 with a thickness of 170 nm, spaced vertically by 500 nm and surrounded by SiO_2. This waveguide geometry increases the effective index of the optical mode as compared to a single strip geometry, which results in higher mode confinement and lower bend loss. The top strip has a width of 1.2 μm and the sidewall angle of the waveguide is between 80° and 82° due to the etching process, which only supports a single mode at 1550 nm and is optimized for coupling of TE polarization. The waveguide has a group index and wavelength dependency of about

Optics EXPRESS

1.72 and 2 × 10^{-5}/nm, respectively. The fabricated filter uses a bend radius of 125 μm to guarantee a low waveguide propagation loss and employs a circuit topology with two ring resonators (one on each arm of the A-MZI) corresponding to a chip size of 10 × 2.5 mm^2 as shown in Fig. 3(b). The circumference of the ring resonators and the MZI inter-arm delay difference are designed to be 1.4 cm and 0.7 cm, respectively, resulting in an FSR of 12.5 GHz for the ring resonator and a FSR of 25 GHz for the A-MZI. The phase shifters are implemented thermo-optically using electrical resistor-based heaters placed on top of the waveguide; the tunable couplers are implemented using MZI couplers with phase shifters in its arms [29,30]. The heaters have an area of 2000 × 20 $μm^2$ for easy fabrication and alignment with waveguides, a tuning speed in the order of milliseconds, and an optical phase shifting efficiency of π/250 mW. In this chip, an average power consumption of about 150 mW/heater is used to compensate the initial circuit parameter offsets and to set the parameters to the target values. An effective measure to reduce the thermo-crosstalk is taken by placing trenches on both sides of the waveguide sections with heaters on top. This suppresses the crosstalk in terms of optical phase shift to less than 5% for a waveguide spacing of 100 μm. The filter has a total insertion loss of 9 dB when accessed using 1550-nm standard single-mode fibers at both ends and having polarization aligned at the input. This includes two times fiber-chip coupling loss about 4 dB/facet (estimated using separate test waveguide structures) and on-chip loss of less than 1 dB with assumption of possible excess loss of the couplers in the circuit. In principle, the fiber-chip coupling efficiency can be further improved by using an optimal taper design of the waveguide facet, which should reduce the coupling loss to about 1 dB/facet [40].

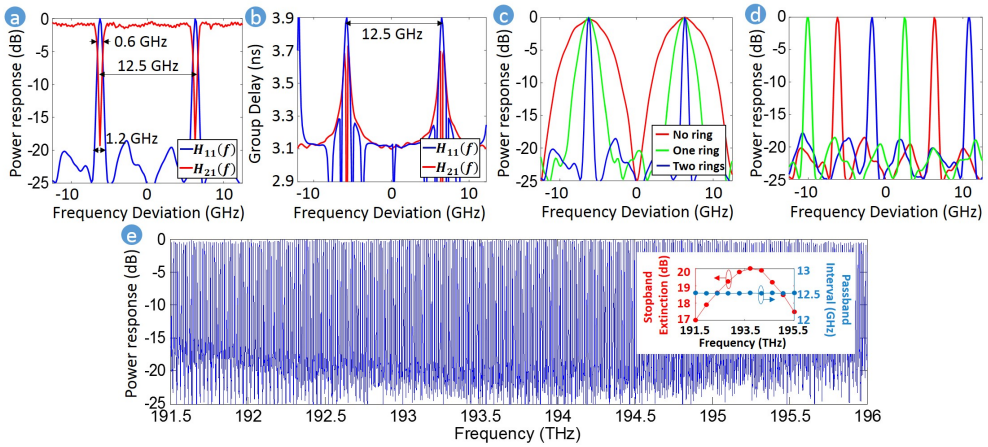

Fig. 4. Measured filter shapes demonstrating: (a, b) the capability of providing both narrow-passband and notch filtering functions, (c) the bandwidth variability of the filter passband, (d) the tuning of passband center frequency, (e) the full C-band coverage of the fabricated chip with an inset showing stopband extinction and passband interval versus wavelength. The responses are normalized to their maximum values.

4. Experiment

The filter shapes measured using an optical vector analyzer (Luna System OVA5000) are shown in Figs. 4(a)–4(e). The tuning elements (filter coefficients) are controlled in accordance to the calculations in Fig. 1. Figures 4(a) and 4(b) show the measured filter shapes and group delays at Port 1 and Port 2, for which the input light was applied to Port 1 via a circulator (AFW Technologies) and both ring resonators were coupled to the A-MZI. The two filter shapes manifest to be a complementary pair, demonstrating the capability of providing both narrow-bandpass and notch filtering functions. For the comb filter application in this work, the narrow-passband filter shape at Port 1 is investigated further. The passbands and

Optics EXPRESS

similar-shaped group delays repeat themselves at a frequency interval of 12.5 GHz. The passband shape features a −3-dB bandwidth of 0.6 GHz and a −20-dB bandwidth of 1.2 GHz, which manifest an excellent frequency selectivity compared with previous demonstrations of similar filter shapes that had FSRs in the order of tens of GHz [35,36,41–47]. An overview of several representative comb filters is shown in Table 2. Figure 4(c) shows the filter shapes obtained when no ring resonator, one ring resonator or both ring resonators were coupled to the A-MZI. This result clearly shows the bandwidth variability of the filter. Figure 4(d) shows the full-range tuning of the center frequency of the filter passbands. This tuning was performed by applying coordinated phase shifts (Table 1) to all phase shifters in the filter simultaneously. The results in Figs. 4(c) and 4(d) demonstrate the reconfigurability of the filter. As another important metric of the filter performance, Fig. 4(e) shows a filter shape measurement with a frequency span of 4.5 THz, i.e. ranging from 191.5 THz to 196 THz. The measurement result shows a nearly constant passband interval of 12.5 GHz and a fluctuation of stopband power extinction of about 3 dB over the complete range. This large bandwidth is accredited to the accurate design, low wavelength dispersion, and excellent waveguide uniformity of the fabricated chip.

Table 2. Overview of several representative comb filters

Ref.	Components	Material	3-dB BW (GHz)	FSR (GHz)	Finesse	>20dB extinction	Loss (dB/cm)	RC	NTE
[41]	RR	SOI	1	50	50	Yes	0.5	Yes	5
[35]	MZI, RR	SOI	0.8	16.5	20.6	Yes	3	Yes	10
[42]	MZI	SOI	1.536	13.5	8.8	No	3	Yes	3
[43]	RR	SOI	2.625	25	9.5	No	6	No	N.A.
[36]	MZI, RR	SOI	3.5	25	7.1	No	6	Yes	7
[44]	MZI, RR	SOI	0.4	10	25	Yes	0.4	Yes	26
[45]	MZI, RR	InGaAsP/InP	3	20	6.7	Yes	5.5	Yes	6
[46]	MZI, RR, SOA	InGaAsP/InP	3.9	26.5	6.8	Yes	N.A.	Yes	21
[47]	MZI, RR, SOA	InGaAsP/InP	1.9	23.5	12.4	Yes	N.A.	Yes	29
This work	MZI, RR	Si_3N_4/SiO_2	0.6	12.5	20.8	Yes	0.1	Yes	5

RR: ring resonator, MZI: Mach-Zehnder interferometer, SOA: semiconductor optical amplifier, RC: reconfigurability, NTE: number of tuning elements

As an application example, we used our comb filter as an external optical clock multiplier. In this experiment, first, an optical clock signal at 1550 nm with a fixed repetition rate of 2.5 Gpulse/s was used as the input to Port 1, which features a 3-dB bandwidth of about 50 GHz and a pulse width of about 10 ps. Figure 5(a) shows the measurements of this pulsed signal in both the frequency (top) and time domains (bottom), where a frequency spacing of 2.5 GHz is observed between the frequency comb lines, associated with a pulse time interval of 400 ps. The filter was configured with two ring resonators coupled to the A-MZI to provide the narrow passband filter shape as shown in Fig. 3(a). Moreover, the filter has its passbands that are frequency-aligned to the comb lines such that each passband allows only one in every five comb lines to pass the filter while suppressing the other four comb lines that are out of the passbands. In effect, the filter performed a sharp spectral selection of frequency comb lines at a frequency spacing of 12.5 GHz, which in the time domain modifies the time interval of the pulses to 80 ps, or equivalently a repetition rate of 12.5 Gpulse/s. Next, we applied another optical clock signal to the filter input, which has a repetition rate of 10 Gpulse/s and a comb spacing of 10 GHz as shown in Fig. 5(b). Likewise, the frequency alignment between the filter passbands and comb lines allows the filter to select one in every five comb lines due to their frequency spacing difference. This filtering results in an output with a comb spacing of

Optics EXPRESS

50 GHz, equivalent to a time domain pulse interval of 20 ps and a repetition rate of 50 Gpulse/s. In our case, however, the bandwidth limitation of the input signal in our laboratory setup allows for only two comb lines in the output, and therefore reduces the output waveform to a Sine shape. This experiment verifies that the critical filter shape of our design enables high-resolution spectral shaping, with a successful demonstration of five-fold repetition rate multiplication of periodically pulsed optical signals, i.e. from 2.5 Gpulse/s to 12.5 Gpulse/s and from 10 Gpulse/s to 50 Gpulse/s.

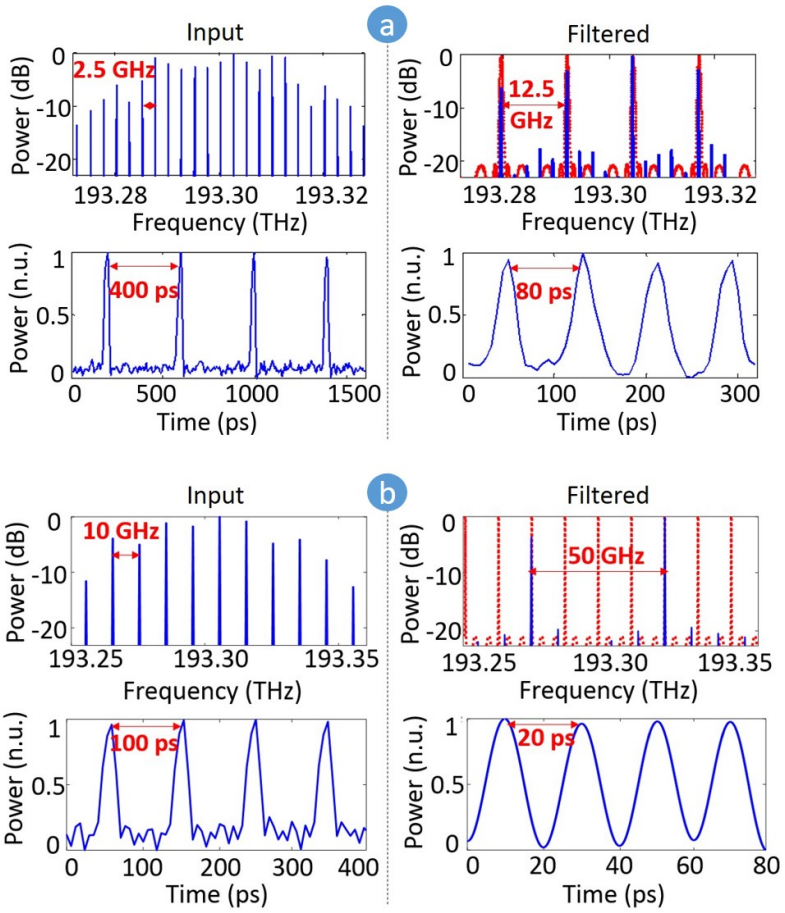

Fig. 5. Demonstration of five-fold repetition rate multiplication of periodically pulsed optical signals: (a) from 2.5 Gpulse/s to 12.5 Gpulse/s, (b) from 10 Gpulse/s to 50 Gpulse/s. The signal spectra were measured using a high-resolution optical spectrum analyzer (Agilent 8164B) and the waveforms were measured using a 50-GHz real-time oscilloscope (Agilent DSO-X 95004Q).

5. Conclusion

The results demonstrated a PIC implementation of an optical clock multiplier. The comb filter function of the proposed circuit topology was experimentally verified, showing a sub-GHz frequency selectivity, i.e. a very narrow passband with a −3-dB bandwidth of 0.6 GHz and a −20-dB bandwidth of 1.2 GHz at a passband interval of 12.5 GHz. This filter shape enables comb spectrum processing (comb line selection) with an order-of-magnitude higher spectral resolution compared with commercial optical filters based on space optics [20,21], and is verified with an experiment of clock rate multiplication, i.e. from 2.5 Gpulses/s to 10

Optics EXPRESS

Gpulses/s and from 10 Gpulses/s to 50 Gpulses/s. For reconfiguring speed and power efficiency, the performance of the tuning elements can be further improved by optimizing heat confinement in the waveguide or by employing other kinds of tuning mechanisms, such as stress-optic modulators [48]. The nearly constant filter passband interval (i.e. nearly constant FSR of the device) across a bandwidth of 4.5 THz verifies excellent control of waveguide length as well as uniformity in fabrication. In this work, we generated the frequency comb by means of a CW laser and external electro-optical modulators, where the frequency alignment with the filter were performed by either tuning the CW laser frequency or on-chip reconfiguring filter passband central frequency (using heaters or adjusting the overall chip temperature). Our experiment used typical open-loop control, but showed good stability of both comb source and filter spectral characteristics. However, frequency locking of the frequency comb would be required for many applications. With this regard, improvements of two aspects can be considered: one is to increase the system robustness by having all of the optical functions monolithically integrated in one chip and packaged with good shielding from ambient disturbances, the second is to develop a close-loop control of the comb and filter frequencies. Moreover, our comb filter can be integrated with many other functions using the same technology, such as delay lines and frequency discriminators [25,26], to create complex chip-scale optical signal processing systems.

Funding

Australian Research Council (ARC) Laureate Fellowship (FL130100041); Australian Research Council's Centre of Excellence CUDOS– Centre for Ultrahigh-bandwidth Devices for Optical Systems (CE110001018).